

# Journal Pre-proof

Discovery of novel NF- $\kappa$ B inhibitor based on scaffold hopping: 1,4,5,6,7,8-hexahydropyrido[4,3-d]pyrimidine

Yue Sun, Zhong-Fei Gao, Wei-Bin Yan, Bin-Rong Yao, Wen-Yu Xin, Chun-Hua Wang, Qing-Guo Meng, Gui-Ge Hou



PII: S0223-5234(20)30336-6

DOI: <https://doi.org/10.1016/j.ejmech.2020.112366>

Reference: EJMECH 112366

To appear in: *European Journal of Medicinal Chemistry*

Received Date: 20 February 2020

Revised Date: 19 April 2020

Accepted Date: 19 April 2020

Please cite this article as: Y. Sun, Z.-F. Gao, W.-B. Yan, B.-R. Yao, W.-Y. Xin, C.-H. Wang, Q.-G. Meng, G.-G. Hou, Discovery of novel NF- $\kappa$ B inhibitor based on scaffold hopping: 1,4,5,6,7,8-hexahydropyrido[4,3-d]pyrimidine, *European Journal of Medicinal Chemistry* (2020), doi: <https://doi.org/10.1016/j.ejmech.2020.112366>.

This is a PDF file of an article that has undergone enhancements after acceptance, such as the addition of a cover page and metadata, and formatting for readability, but it is not yet the definitive version of record. This version will undergo additional copyediting, typesetting and review before it is published in its final form, but we are providing this version to give early visibility of the article. Please note that, during the production process, errors may be discovered which could affect the content, and all legal disclaimers that apply to the journal pertain.

© 2020 Published by Elsevier Masson SAS.

## Table of Contents Graphic and Synopsis

Discovery of novel NF- $\kappa$ B inhibitor based on scaffold hopping:1,4,5,6,7,8-hexahydropyrido[4,3-*d*]pyrimidine

Yue Sun <sup>a</sup>, Zhong-Fei Gao <sup>a</sup>, Wei-Bin Yan <sup>a</sup>, Bin-Rong Yao <sup>a</sup>, Wen-Yu Xin <sup>a</sup>, Chun-Hua Wang <sup>a,\*\*\*</sup>, Qing-Guo Meng <sup>b,\*\*</sup>, Gui-Ge Hou <sup>a,\*</sup>

<sup>a</sup> School of Pharmacy, the Key Laboratory of Prescription Effect and Clinical Evaluation of State Administration of Traditional Chinese Medicine of China, Binzhou Medical University, Yantai, 264003, P. R. China.

<sup>b</sup> School of Pharmacy, Key Laboratory of Molecular Pharmacology and Drug Evaluation (Yantai University), Ministry of Education, Collaborative Innovation Center of Advanced Drug Delivery System and Biotech Drugs in Universities of Shandong, Yantai University, Yantai 264005, People's Republic of China.

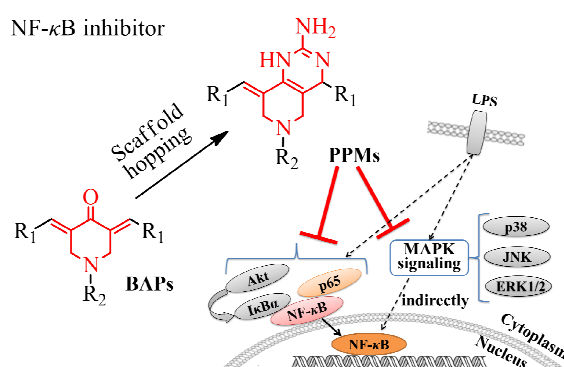
\* Corresponding authors.

\*\* Corresponding authors.

\*\*\* Corresponding authors.

E-mail addresses: *guigehou@163.com* (G.-G. Hou), *qinggmeng@163.com* (Q.-G. Meng), *chunhuawang508@126.com* (C.-H. Wang)

Fluoro-substituted 1,4,5,6,7,8-hexahydropyrido[4,3-*d*]pyrimidines (PPMs) were synthesized based on scaffold hopping. PPM **43** substituted by 3-F and 4-CF<sub>3</sub> groups could be the most potent NF- $\kappa$ B inhibitor, because it induced dose-dependent cell apoptosis at cell and protein level, while inhibited NF- $\kappa$ B activation by suppressing LPS-induced phosphorylation and nuclear translocation of NF- $\kappa$ B signaling.



**Discovery of novel NF- $\kappa$ B inhibitor based on scaffold hopping:****1,4,5,6,7,8-hexahydropyrido[4,3-*d*]pyrimidine**

Yue Sun <sup>a</sup>, Zhong-Fei Gao <sup>a</sup>, Wei-Bin Yan <sup>a</sup>, Bin-Rong Yao <sup>a</sup>, Wen-Yu Xin <sup>a</sup>, Chun-Hua Wang <sup>a,\*\*\*</sup>, Qing-Guo Meng <sup>b,\*\*</sup>, Gui-Ge Hou <sup>a,\*</sup>

<sup>a</sup> School of Pharmacy, the Key Laboratory of Prescription Effect and Clinical Evaluation of State Administration of Traditional Chinese Medicine of China, Binzhou Medical University, Yantai, 264003, P. R. China.

<sup>b</sup> School of Pharmacy, Key Laboratory of Molecular Pharmacology and Drug Evaluation (Yantai University), Ministry of Education, Collaborative Innovation Center of Advanced Drug Delivery System and Biotech Drugs in Universities of Shandong, Yantai University, Yantai 264005, People's Republic of China.

\* Corresponding authors.

\*\* Corresponding authors.

\*\*\* Corresponding authors.

E-mail addresses: *guigehou@163.com* (G.-G. Hou), *qinggmeng@163.com* (Q.-G. Meng), *chunhuawang508@126.com* (C.-H. Wang)

**Authors' contributions:**

G.-G. Hou, and C.-H. Wang designed the research and wrote the paper.

Y. Sun and Z.-F. Gao synthesized and characterized PPMs derivatives.

Y. Sun, W.-B. Yan, and B.-R. Yao performed the experiments related to the biological effects.

Q.-G. Meng performed the Molecular docking and discussion.

W.-Y. Xin provided scientific direction related to the biological experiments.

## Abbreviations

NF- $\kappa$ B, nuclear factor-TNF- $\alpha$ ;

PPMs, 1,4,5,6,7,8-hexahydropyrido[4,3-*d*]pyrimidines;

BAPs, 3,5-bis(arylidene)-4-piperidones;

LPS, Lipopolysaccharides;

HCC, Hepatocellular carcinoma;

TNF- $\alpha$ , tumor necrosis factor- $\alpha$ ;

NO, Nitric oxide;

IKK, inhibitor of TNF- $\alpha$  kinase;

EDC, 1,2-dichloroethane;

EtOH, Ethanol;

MeOH, Methanol;

DOX, Doxorubicin;

DMSO, Dimethyl sulfoxide;

DCM, Dichloromethane;

**Abstract:** NF- $\kappa$ B is a key signaling pathway molecule linking hepatoma and chronic inflammation. Inhibition of NF- $\kappa$ B activation can alleviate inflammation, and promote hepatoma cell apoptosis. In this study, a series of fluoro-substituted 1,4,5,6,7,8-hexahydropyrido[4,3-*d*]pyrimidines (PPMs, **31-57**) were synthesized from 3,5-bis(arylidene)-4-piperidones (BAPs, **4-30**) based on scaffold hopping. We successfully discovered the most potent **43** substituted by electron-withdrawing substitutes (3-F and 4-CF<sub>3</sub>) exhibited less toxicity and higher anti-inflammatory activity. Preliminary mechanistic studies revealed that **43** induced dose-dependent cell apoptosis at cell and protein level, while inhibited NF- $\kappa$ B activation by suppressing LPS-induced phosphorylation levels of p65, I $\kappa$ B $\alpha$  and Akt, and by indirectly suppressing MAPK signaling, and by inhibiting the nuclear translocation of NF- $\kappa$ B induced by TNF- $\alpha$  or LPS. Docking analysis verified simulated **43** could reasonably bind to the active site of Bcl-2, p65 and p38 proteins. This compound, as a novel NF- $\kappa$ B inhibitor, also demonstrated both anti-inflammatory and anti-hepatoma activities, warranting its further development as a potential multifunctional agent for the clinical treatment of liver cancers and inflammatory diseases.

**Keywords:** NF- $\kappa$ B inhibitor; 1,4,5,6,7,8-hexahydropyrido[4,3-*d*]pyrimidines; 3,5-bis(arylidene)-4-piperidones; scaffold hopping; anti-hepatoma; anti-inflammatory

## 1. Introduction

Liver cancer is the seventh most commonly diagnosed cancer and the third leading cause of cancer related deaths worldwide in 2018 [1]. It claims more than 841080(4.7%) lives per year and the global death toll 781631(8.2%) continues to increase [1]. There are the highest incidence and mortality of liver cancer in China, accounting for about 20% of the new cases and deaths worldwide [2]. Hepatocellular carcinoma (HCC) is the most frequent type of primary liver cancer, accounting for about 80% of such incidences [3]. The nuclear factor  $\kappa$ B (NF- $\kappa$ B) is a key signaling pathway molecule linking HCC and chronic inflammation [4,5].

The mammalian NF- $\kappa$ B is a protein complex, which encompasses five members, including p50, p52, p65 (RelA), RelB, and c-Rel. Under normal physiological conditions, NF- $\kappa$ B combined with inhibiting protein I $\kappa$ B into a dimer, which was in a state of deactivation. After stimulation from various proinflammatory cytokines, chemokines, and other mediators such as tumor necrosis factor (TNF)- $\alpha$ , and nitric oxide (NO), I $\kappa$ B kinase (IKK) was activated and I $\kappa$ B was phosphorylated predominately, which made the protein p65 release. This releases NF- $\kappa$ B dimer and allows it to translocate into the nucleus to activate specific target genes [6,7].

From the formation process of chronic inflammation to HCC, inflammatory cytokines (TNF- $\alpha$ , IL-1, IL-6, IL-17, COX-2) can mediate NF- $\kappa$ B activation [8,9]. Whereas, NF- $\kappa$ B excessive activation can block HCC cell apoptosis, and trigger malignant cell proliferation. In the stage of liver cancer growth and metastasis, NF- $\kappa$ B sustained activation leads to increased resistance of tumor cells [10,11]. Inhibition of NF- $\kappa$ B activation can alleviate inflammation, and promote HCC cell apoptosis [12,13]. To date, there is no ideal drugs that are targeted NF- $\kappa$ B for treatment of HCC. Therefore, developing novel NF- $\kappa$ B inhibitors and exploring the mechanism of anti-hepatoma are of great theoretical significance.

Curcumin (Fig. 1.) has anti-inflammatory, anti-tumor, anti-oxidation and other activities. But its clinical application is limited because of its low stability, poor bioavailability and false positive [14]. So structural modification based on curcumin was carried out and large amounts of curcumin analogues have been reported. Therein, (3*E*, 5*E*)-3,5-bis(arylene)-4-piperidones

(BAPs, Fig. 1.) was a very distinguished class because they could inhibit tumor growth by anti-inflammatory and inhibiting NF- $\kappa$ B dependent signaling pathways [15,16].

In our group, some symmetric and dissymmetric BAPs as antitumor and anti-inflammatory agents were designed and synthesized [17-23], which exhibited both an antitumor and anti-inflammatory activity by prominently inhibiting the activation of NF- $\kappa$ B signal pathway by blocking the phosphorylation of I $\kappa$ B $\alpha$ , p65 and the nuclear translocation of NF- $\kappa$ B [17,18, 23]. However, the water-solubility and toxicity should be further optimized.

In our study, alternative scaffold hopping strategy [24-26] was applied to discover novel NF- $\kappa$ B inhibitors that could inhibit NF- $\kappa$ B activation. We started with the structural characteristics of BAPs, and found that central  $\alpha,\beta$ -unsaturated ketones of BAPs could condense with guanidine hydrochloride to generate 1,4,5,6,7,8-hexahydropyrido[4,3-*d*]pyrimidine (PPMs) based on scaffold hopping (Fig. 1.). According to literatures, PPMs were rarely documented [27-30]. Our efforts led to the discovery of fluorine-substituted BAPs and PPMs, and evaluated as potential NF- $\kappa$ B inhibitors for further clinical treatment of liver cancer.

**Fig. 1**

## **2. Results and Discussion**

### ***2.1. Synthesis and Structural characterization of BAPs and PPMs***

The synthetic routes of BAPs and PPMs are shown in Scheme 1. The described methods of their preparation include Claisen-Schmidt condensation, *N*-sulfonylation, and Michael addition reactions. Firstly, *o*-, *m*-, and *p*-fluorine-substituted intermediates **3** in the form of hydrochloride were obtained through Claisen-Schmidt condensation between **1** and **2** [17,18]. Secondly, they were used to synthesize *N*-phenylsulfonyl-BAPs (BAPs, **4-30**) by *N*-sulfonylation reaction between **3** and benzene sulfonyl chlorides with different substituents, such as R<sub>2</sub> = -H, -Me, -NO<sub>2</sub>, -CF<sub>3</sub>, -X, -CN, -NHAc. In this reaction, pyridine was used as a catalyst and acid-binding agent, which can neutralize HCl from compound **3** and the *N*-sulfonylation reaction. Thirdly, an efficient synthesis of

1,4,5,6,7,8-hexahydropyrido[4,3-*d*]pyrimidine derivatives (PPMs, **31-57**) were carried out by the reaction of BAPs and guanidine hydrochloride under base catalysis. To the best of our knowledge, PPMs displayed various remarkable biological activities, such as antibacterial, antiallergic, antiviral, and anti-inflammatory property, however, there were no more than twenty PPMs in the literatures [27-30]. Herein, a variety of *N*-phenylsulfonyl-BAPs (**4-30**), possessing electron-withdrawing groups (*o*-, *m*-, or *p*-fluorine) were employed for PPMs formation because electron-withdrawing groups on the phenyl rings could induce greater electronic positive charge on the corresponding atoms and accelerate the process of condensation reaction [29]. In this condensation reaction, the presence of a base (Potassium hydroxide or Potassium carbonate) is essential to provide a basic conditions resulting in Michael addition between guanidine hydrochloride and BAPs. After elimination of water, target products (PPMs **31-57**) obtained. After optimization of the reaction conditions, Michael addition reaction can be completed under 1.5~3 hours, while EDC/EtOH reaction system was superior to EDC/MeOH reaction system because the former can withstand higher reaction temperatures. The yields were between 73% and 88%. All PPMs were characterised by  $^1\text{H}$  NMR,  $^{13}\text{C}$  NMR, IR and HRMS-ESI, and all data are described in Supporting Information.

### Scheme 1

Take BAP **17** and PPM **44** as examples. Compared with  $^1\text{H}$  NMR spectrum of **17** (Fig. 2B), four evident unimodal signals in 10.50, 9.21, 7.81, and 5.27 ppm can be found, which are attributed to five proton signals of -NH, -NH<sub>2</sub> and -CH in 1,4,5,6,7,8-hexahydropyrido[4,3-*d*]pyrimidine of **44** (Fig. 2A). Refer to a literature report [31], there are two -NH proton signals, therefore we presume that compound should be in the form of hydrochloride. In  $^{13}\text{C}$  NMR spectra of **44** (Fig. 2C), the corresponding carbon atoms of methyne appear in 54.00 ppm chemical shift, whereas there is no carbon signal of methyne in Fig. 2D. In addition, there is a single-peak in 4.69 ppm (Fig. 2B), which is corresponding to the proton signals of the methylene groups in central piperidone. After changing **17** to **44**, the methylene signals split into four doublets (Fig. 2A) with coupling constants values ranging of 16-18 Hz, as a result of the Geminal Coupling of axial and equatorial hydrogens of two different methylene groups in the 1,4,5,6,7,8-hexahydropyrido[4,3-*d*]pyrimidine ring.

Similarly, double carbon signals of two methylene groups with different electronic environment of **44** appear in different chemical shift (44.85 and 44.55 ppm) in  $^{13}\text{C}$  NMR spectra (Fig. 2C). In addition, molecular formula of **44** was established as  $\text{C}_{26}\text{H}_{22}\text{ClF}_3\text{N}_4\text{O}_2\text{S}$  by HRMS-ESI at  $m/z$  511.1424  $[\text{M}+\text{H}]^+$  (calcd. for  $\text{C}_{26}\text{H}_{22}\text{F}_3\text{N}_4\text{O}_2\text{S}^+[\text{M}+\text{H}]^+$ , 511.1416).

**Fig. 2.**

To further confirm the structure, the single crystals of PPM **49** were obtained through evaporation from a DCM and MeOH solution. The ORTEP diagram of **49** is presented in Fig. 3A. **49** crystallizes in the monoclinic and chiral space group  $P 2_1$ . The asymmetric unit contains one pharmaceutical molecule and a MeOH molecule. As shown in Fig. 3A, both nitrogen atoms of central 1,4,5,6,7,8-hexahydropyrido[4,3-*d*]pyrimidine unit form two group of N-H. It's basically the same bond length, and  $d_{\text{C1-N1}}$ ,  $d_{\text{C1-N2}}$  and  $d_{\text{C1-N3}}$  are 1.342(5) Å, 1.328(5) Å and 1.323(6) Å, respectively. Meanwhile, there is a chloride ion. As suggested by the analysis of  $^1\text{H}$  NMR spectrum, compound **49** exists in the form of hydrochloride in crystalline state, which is consistent with a literature report [31]. Structurally, C2 atom adopts *S* configuration, and *p*-fluorophenyl group and 1,4,5,6,7,8-hexahydropyrido[4,3-*d*]pyrimidine are almost vertical, which dihedral angle is  $86.363(4)^\circ$ . In addition, the *N*-phenylsulfonyl group extends in the same direction as the amino group of **49**, which dihedral angle is  $29.256(3)^\circ$ .

**Fig. 3.**

## 2.2. *In vitro* cytotoxicity, anti-inflammatory activity and structure-activity relationship (SAR) analysis

In the previous study, BAPs with electron-withdrawing groups (-F, -CF<sub>3</sub>, such as BAP **6d** [19], BAP **67** [17], EF24 [32,33], as shown in Fig. 3B) in the additional binding site C (Fig. 1) demonstrated the most potent bioactivities, while *N*-benzenesulfonyl-BAPs can improve cytotoxicity and reduce toxicity than *N*-methyl-BAPs in the additional binding site B (Fig. 1) of BAPs [17,18]. Therein, fluorine substituents of drugs play an important role in bioactivities [34], which lipophilicity can effectively improve the membrane permeability of drugs; Fluorine atom, as a strong electronegative group, can form multiple H-bonds with target protein; In addition, stable C-F bond can improve metabolic stability and thus prolongs

duration of action *in vivo*. Inspired by the interesting bioactivity, *o*-, *m*-, and *p*-fluorine-substituted BAPs (**4-30**) were prepared and selected to screen for bioactivity in spite of **8** and **12** (Fig. 3B) which structures were reported in our previous study [18]. The *N*-phenylsulfonyl substituents contain great electron-donating substituents (-Me, -NHAc) or electron-withdrawing substituents (-NO<sub>3</sub>, -CF<sub>3</sub>, -X, and -CN) as shown in Table 1. Human HCC cell lines (HepG2, SMMC-7721) and non-malignant cell lines (HHL-5 and LO2) were selected to evaluate cytotoxicity by MTT assay. DOX was used as a positive control.

**Table 1**

For *o*-fluorine-substituted **4-12**, *N*-phenylsulfonyl-substituted **4** have IC<sub>50</sub> values greater than 5.0 μM for HepG2 and SMMC-7721 cells, and greater than 15.0 μM for HHL-5 and LO2 cells. This showed that **4** displayed lower cytotoxicity. After substituent of other substituents, 4-CF<sub>3</sub>-substituted **7** displayed better cytotoxicity against HepG2 (4.9 μM) than that of **4**, and 4-Me-substituted **5** or 4-Cl-substituted **9** displayed better cytotoxicity against SMMC-7721 cells than **4**. However, toxicity of **5**, **7** and **9** toward HHL-5 and LO2 was also significantly increased, and similar to that of DOX. For *m*-fluorine-substituted **13-21**, their cytotoxicity has improved greatly compared with *o*-fluorine-substituted BAPs. The IC<sub>50</sub> values of **13**, **14**, **16**, and **20** against HepG2 were lower than 5.0 μM (3.4 μM, 3.5 μM, 2.4 μM, and 2.6 μM, respectively). The IC<sub>50</sub> values of **16** and **20** against SMMC-7721 were only 4.2 μM and 4.5 μM. This results showed BAPs substituted by stronger electron-withdrawing substituents (-CF<sub>3</sub> (**16**), -CN (**20**)) can led to more potent cytotoxicity against HCC cells in spite of bigger toxicity toward non-malignant cell lines. For *p*-fluorine-substituted **22-30**, 4-CF<sub>3</sub>-substituted **25** demonstrated accredited cytotoxicity against HepG2 and SMMC-7721 (3.2 μM and 4.4 μM, respectively). 4-Me-substituted **23** or 4-Cl-substituted **27** displayed better cytotoxicity against HepG2 cells. Similar to the previous two series, *p*-fluorine-substituted BAPs displayed slightly higher toxicity toward HHL-5 and LO2.

Through analysis of the substituent effect of BAPs, the end of *N*-phenylsulfonyl group was substituted by stronger electron-withdrawing substituents (Such as -CF<sub>3</sub>, -CN) resulting in more potent cytotoxicity against three HCC cells. It's even more unfortunate that their cytotoxicity were all weaker than DOX, while toxicity were comparable to DOX. Previous

studies have shown that BAPs exhibited both an antitumor and anti-inflammatory activity by prominently inhibiting the activation of NF- $\kappa$ B signal pathway [17,18, 23], whereas greater toxicity will limit its use as a NF- $\kappa$ B inhibitor. In order to optimize their bioactivity and discover novel NF- $\kappa$ B inhibitors, alternative scaffold hopping strategy was applied to change BAPs (**4-30**) to PPMs (**31-57**) by Michael addition reactions. Their IC<sub>50</sub> values are shown in Table 2.

**Table 2**

For *o*-fluorine-substituted PPMs **31-39**, 4-CF<sub>3</sub>-substituted **34** displayed better cytotoxicity against HepG2 (3.9  $\mu$ M) and SMMC-7721 (3.5  $\mu$ M) than that of BAP **7**. While 4-Cl-substituted **36** has equivalent IC<sub>50</sub> value against SMMC-7721 with BAP **9**. It is interesting that the toxicity toward HHL-5 and LO2 has great improvement, which can be proved by their IC<sub>50</sub> value (20.8  $\mu$ M toward HHL-5, and 22.0  $\mu$ M toward LO2 for PPM **34**). However, cytotoxicities of **31-33**, **35**, **37-39** were not too optimistic. For *m*-fluorine-substituted **40-48**, *N*-phenylsulfonyl-substituted **40** have a lower IC<sub>50</sub> values (3.7  $\mu$ M) than 5.0  $\mu$ M against HepG2, but the IC<sub>50</sub> values (12.8  $\mu$ M) against SMMC-7721 for **40** was higher than that against HepG2. Compared with BAP **13**, cytotoxicity of **40** was not significantly improved. Nevertheless, PPMs **43**, **44**, **47** substituted by electron-withdrawing substitutes (-CF<sub>3</sub>, -F, -CN) led to potent cytotoxicity against HCC cells. Especially for 4-CF<sub>3</sub>-substituted PPM **43** displayed the most potent cytotoxicity. The IC<sub>50</sub> values against HepG2, SMMC-7721 of **43** are only 2.1  $\mu$ M, 2.4  $\mu$ M, respectively, which cytotoxicity was greatly improved from **16**. More importantly, toxicity of **43** toward HHL-5 and LO2 (28.8  $\mu$ M and 35.2  $\mu$ M) are significantly lower than **16** and DOX. For *p*-fluorine-substituted **49-57**, PPMs **50**, **52**, **53** with lower IC<sub>50</sub> values show potential cytotoxicity against HCC cells. Therein, their IC<sub>50</sub> values against HepG2, SMMC-7721 of **50** and **52** are approximately the same as that of **23** and **25**, respectively, but toxicity of **50** and **52** have significant improvement compared **23** and **25**. The cytotoxicity of **53** against HepG2 doubled from **26**, and their IC<sub>50</sub> value changed from 8.1  $\mu$ M to 4.1  $\mu$ M. Integrating the previous discussion, PPMs with electron-withdrawing groups (**34**, **43**, **44**, **47**, **52** and **53**) exhibited more potential cytotoxicity to HCC cells and lesser toxicity to normal cells HHL-5 and LO2, especially

which revealed that electron-withdrawing substitutes (-CF<sub>3</sub>, -F) could improve the bioactivity.

**Table 3**

All PPMs were tested for their anti-inflammatory activity by ELISA method. Pre-experimental results displayed all BAPs and PPMs had no obvious toxicity to RAW264.7 cells at 5.0 μM (Supporting Information).

LPS has been used to induce an inflammatory response in experimental cells, which could lead to the activation of intracellular signaling pathways and transcription factors, and subsequently induce the production of inflammatory mediators, including IL-6 and TNF-α [35,36]. In our study, the inhibition rates of IL-6 and TNF-α cytokine release in LPS-stimulated RAW264.7 macrophages are shown in Table 3. For *o*-fluorine-substituted PPMs (**31-39**), 4-substituted **34** (4-CF<sub>3</sub>) and **36** (4-Cl) displayed higher inhibition rates against IL-6 and TNF-α cytokine release at a concentration of 5.0 μM. They can be more than 80%. While 4-substituted **33** (4-NO<sub>2</sub>), **35** (4-F), and **37** (4-Br) have medium inhibition rates against cytokine release, and they can reach 70%. After changed substituents from *o*-F to *m*-F (PPMs, **40-48**), only **43** (4-CF<sub>3</sub>), **44** (4-F), and **47** (4-CN) exhibited significant anti-inflammatory activity, whose inhibition rates were reach about 88.5%, 71.6%, 74.5% for TNF-α, and 86.8%, 74.9%, 73.0% for IL-6, respectively. For *p*-fluorine-substituted **49-57**, inhibition rates of **52** (4-CF<sub>3</sub>) and **53** (4-F) can be higher than 70%. Intriguingly, among them, inhibition rates of **34**, **36**, **43**, and **52** by inhibiting TNF-α and IL-6 cytokines release at a concentration of 5.0 μM are more than 80%, which exhibited more significant anti-inflammatory activity than PDTTC. Comparatively, the inhibition rates followed the order **43** (88.5%) > **52** (87.5%) > **34** (84.4%) > **36** (83.0%) by inhibiting TNF-α release, while **43** (86.8%) > **34** (82.3%) > **52** (81.7%) > **36** (81.5%) by inhibiting IL-6 release under 5.0 μM concentration.

Combined with previously discussed cytotoxicity, it is obvious to find that PPMs (**34**, **43**, and **52**) substituted by electron-withdrawing substitutes (-CF<sub>3</sub>) have the better cytotoxicity, less toxicity and more significant anti-inflammatory activity. The cytotoxicity against HCC cells followed the order **43** (average, 2.3 μM) > **52** (average, 3.6 μM) > **34** (average, 3.7 μM), while toxicity to normal cells HHL-5 and LO2 followed the order **43** (average, 32.0 μM) > **34** (average, 21.4 μM) > **52** (average, 19.9 μM), indicating that the position of -F groups could affect the activity. Among them, **43** should be the most potential compound, which can be used as a lead compound for subsequent research. The structure of **43** is shown in Fig. 4A.

### **2.3. PPM 43 induced HCC cells apoptosis in a dose-dependent manner**

In order to understand the anti-hepatoma mechanism of PPMs, the experiments of reducing cell apoptotic of HepG2 and SMMC-7721 by **43** were carried out through flow cytometry. As shown in Fig. 4B, **43** (1.0  $\mu\text{M}$ ) could induce 63.9% apoptosis for HepG2 cells, and 18.3% apoptosis in SMMC-7721 cells, respectively. Under 4.0  $\mu\text{M}$ , rate of cells apoptosis could reach 68.3% (HepG2) and 20.6% (SMMC-7721), which showed that **43** induced HCC cell apoptosis in a dose-dependent manner, while the effect for HepG2 was more significant than that for SMMC-7721.

At the protein level, cell apoptotic proteins (BAX, Bcl-2, and C-Caspase-3) also play a key role in cancer cell apoptosis [37]. HepG2 cells were selected for western blot experiment of **43** under the concentration of 1.0, 2.0, 4.0  $\mu\text{M}$ . As shown in Fig. 4C, the protein expression of pro-apoptotic BAX and C-Caspase-3 significantly increased, while the protein expression of anti-apoptotic Bcl-2 significantly reduced. More importantly, **43** can dose-dependently regulate the protein expression to induce apoptosis of HepG2 cells. Combined with the results of flow cytometry and western blot, it was concluded that **43** could induce cell apoptosis at cell level and protein level and in a dose-dependent manner.

**Fig. 4.**

***PPM 43 inhibited the phosphorylation of I $\kappa$ B and p65 in HepG2 cells***

NF- $\kappa$ B is a key signaling pathway molecule linking hepatoma and chronic inflammation [6]. Excessive NF- $\kappa$ B activation can contribute to the pathogenesis of hepatoma and chronic inflammation. Based on aforementioned cellular results, we continue to explore the molecular mechanism by which **43** inhibited NF- $\kappa$ B signaling. After LPS stimulation in RAW 264.7 cells, related Akt/I $\kappa$ B pathway, IKK/I $\kappa$ B pathway and mitogen-activated protein kinase (MAPK) pathway will be activated [12]. Therefore, we can inhibit the phosphorylation of these key regulators to regulate NF- $\kappa$ B signaling pathway by **43**, which was investigated by Western blotting (Fig. 5A).

In our study, LPS (1.0  $\mu\text{g}/\text{mL}$ ) can significantly cause phosphorylation of p65 and I $\kappa$ B $\alpha$  in RAW264.7 cells at 30 min. After treatment with different concentrations (1.0, 2.0, 4.0  $\mu\text{M}$ ) of **43**, the phosphorylation levels of p65 and I $\kappa$ B $\alpha$  were significantly reduced, and the inhibition of phosphorylation became more pronounced as the concentration increased (Fig.

5C and 5D). These results showed that **43** could inhibit NF- $\kappa$ B activation by inhibiting phosphorylation levels of p65 and I $\kappa$ B $\alpha$ . Then, the upstream signaling event for Akt activation was investigated. The effect of **43** on the LPS-induced phosphorylation of Akt was shown in Fig. 5B. LPS induced the phosphorylation of Akt in RAW264.7 cells and the induction was markedly attenuated by **43**, indicating that **43** can inhibit NF- $\kappa$ B activation via inhibiting phosphorylation levels of Akt.

It is well-known that MAPKs are the key signaling adaptors in the LPS-induced macrophages [38]. To determine whether **43** could affect the MAPK signaling pathway, the phosphorylation levels of p38, extracellular signal regulated protein kinase (ERK) and c-Jun N-terminal kinase (JNK) were examined. After LPS treatment, the phosphorylation levels of three factors of MAPKs at 30 min (Fig. 6A). Then RAW264.7 cells were treated with different concentrations (1.0, 2.0, 4.0  $\mu$ M) of **43**, the expression levels of LPS-induced p-p38, p-ERK and p-JNK were decreased to different degrees (Fig. 6B-6D). The results suggested that **43** also can indirectly inhibit NF- $\kappa$ B activation via the MAPK signaling.

On the basis of these results, we proposed a putative mechanism for **43** inhibition on NF- $\kappa$ B signaling. Briefly, **43** might inhibit NF- $\kappa$ B activation by inhibiting phosphorylation levels of p65, I $\kappa$ B $\alpha$  and Akt, and by indirectly suppressing MAPK signaling, eventually leading to downregulation of inflammatory mediators.

**Fig. 5.**

**Fig. 6.**

#### ***2.4. PPM 43 prevented P65 nuclear translocation induced by LPS or TNF- $\alpha$ .***

To better understand the inhibitory effect of LPS- or TNF- $\alpha$ -induced NF- $\kappa$ B activation by **43**, p65 nuclear translocation in HepG2 and RAW264.7 cells can be determined by immunofluorescence. Using DMSO as a control group, the results show that most of p65 protein can detect in cytoplasm of RAW264.7 or HepG2 cells (Fig. 7). After stimulation with LPS (1.0  $\mu$ g/mL) or TNF- $\alpha$  (10 ng/mL), the majority of p65 nuclear translocations can be found in experimental cells. If pre-treatment of cells with **43** (4.0  $\mu$ M) together, p65 nuclear translocation was effectively prevented. The p65 protein was mainly detected in the cytoplasm other than cell nucleus. In general, **43** probably inhibit NF- $\kappa$ B activation by prevent

LPS- or TNF- $\alpha$ -induced p65 nuclear translocations in RAW264.7 or HepG2 cells. In other word, **43** could inhibit NF- $\kappa$ B activation to display potential anti-inflammatory and anti-hepatoma activities.

**Fig. 7.**

### **2.5. The molecular docking**

Further explore the interaction between **43** and Bcl-2, NF- $\kappa$ B/p65, and p38 proteins, molecular docking was performed in LibDock of Discovery Studio 2017R2. The crystal structures of Bcl-2 (PDB: 1YSW), p65 (PDB: 1MY5), and p38 (PDB: 4FA2) proteins were obtained from Protein Data Bank. After removing original ligands, optimized proteins were set as receptors and placed the optimized 3D molecule of **43** in the sphere position for molecular docking [39]. The 3D and 2D models between simulated **43** and the active site of proteins were generated.

As shown in Fig. 8A, 4-(trifluoromethyl)benzenesulfonyl and *m*-fluorophenyl groups of simulated **43** could insert into two lipophilic pockets of Bcl-2 protein, while central 1,4,5,6,7,8-hexahydropyrido[4,3-*d*]pyrimidine crosses the narrow and shallow channel by  $\pi$ -anion interactions.

As shown in Fig. 8B, *m*-fluorophenyl groups of **43** crosses the channel of p65 protein through  $\pi$ -anion and amide- $\pi$  stacked interactions. In addition, 4-(trifluoromethyl)benzenesulfonyl groups attach to the surface of p65 protein through halogen and  $\pi$ -anion interactions. Interestingly, central 1,4,5,6,7,8-hexahydropyrido[4,3-*d*]pyrimidine plays an important role in binding to p65 protein. There are stronger hydrogen bonds between 2-aminopyrimidine and hinge residues (Ler262, Asp291). Unfortunately, no significant interactions can be found in another *m*-fluorophenyl group of **43** with Bcl-2 and p65 proteins.

Molecular docking between **43** and p38 protein is shown in Fig. 8C. Under the bridged action of 1,4,5,6,7,8-hexahydropyrido[4,3-*d*]pyrimidine of **43**, 4-(trifluoromethyl)benzenesulfonyl and *m*-fluorophenyl groups bend to one side, which looks like a organic clip [40]. This clip exactly insert into the big pocket of p38 protein through very

complex interactions, which can be seen in 2D models of Fig. 8C. It is different from Bcl-2 and p65 proteins that another *m*-fluorophenyl group of **43** can reasonably bind to superficial hinge residues of p38 protein.

Based on the above docking analysis, simulated **43** could reasonably bind to the active site of Bcl-2, p65 and p38 proteins. The results of molecular docking are basically consistent with aforementioned discussion of western blot. This theoretically explains in detail why **43** has potential anti-inflammatory and anti-hepatoma activities.

**Fig. 8.**

### 3. Conclusions

NF- $\kappa$ B plays an essential role at the crossroad of liver cancer and inflammation, which can effectively regulate a number of cellular activities. Especially, its aberrant activation could induce pathogenesis of HCC, for example, block HCC cell apoptosis and trigger malignant cell proliferation. Developing novel small-molecule agents through inhibiting NF- $\kappa$ B activation would provide potential therapeutics for the treatment of liver cancer by both anti-hepatoma and anti-inflammatory activities. In our previous study, BAPs exhibited both antitumor and anti-inflammatory activities by prominently inhibiting NF- $\kappa$ B activation, whereas water-solubility and toxicity of BAPs were not optimistic. We utilized the strategy of alternative scaffold hopping to discover novel potential NF- $\kappa$ B inhibitors for further clinical treatment of liver cancer. A series of fluoro-substituted PPMs were generated from BAPs based on scaffold hopping. Structural modification and SAR studies of all PPMs led to successful discovery of the most potent PPM **43** substituted by electron-withdrawing substitutes (3-F and 4-CF<sub>3</sub>). It exhibited better anti-hepatoma activities, less toxicity and higher anti-inflammatory activity. Preliminary mechanistic studies revealed that **43** could induce cell apoptosis at cell level and protein level and in a dose-dependent manner. More importantly, **43** effectively inhibited NF- $\kappa$ B activation by suppressing LPS-induced phosphorylation levels of p65, I $\kappa$ B $\alpha$  and Akt, and by indirectly suppressing MAPK signaling. In addition, **43** could inhibit NF- $\kappa$ B activation by prevent LPS- or TNF- $\alpha$ -induced p65 nuclear translocations in RAW264.7 or HepG2 cells. Docking analysis verified simulated **43** could

reasonably bind to the active site of Bcl-2, p65 and p38 proteins. Herein, we obtained a novel NF- $\kappa$ B inhibitor with great potential for further development as multifunctional therapeutic agent for the clinical treatment of liver cancers and inflammatory diseases.

## 4. Materials and Methods

### 4.1. Chemistry

4-Piperidinone hydrate hydrochloride (**1**), aromatic aldehyde (**2**), benzenesulfonyl chloride and guanidine hydrochloride are all from Sinopharm Holding Chemical Reagent Co., Ltd. (Shanghai, China) and do not require further purification. Infrared (IR) spectra were obtained in the 400-4000  $\text{cm}^{-1}$  range using a Perkin-Elmer Frontier Mid-IR FTIR Spectrometer.  $^1\text{H}$  NMR data were collected using a Bruker Avance 400 or 600 MHz.  $^{13}\text{C}$  NMR data were collected at 100 MHz on a Bruker Avance 400 MHz spectrometer or 150 MHz on a Bruker Avance 600 MHz spectrometer. Chemical shifts were reported in  $\delta$  relative to TMS. The HRMS-ESI data were obtained on a Finnigan-MAT-95 mass spectrometer. All melting points were measured on a digital melting point apparatus and were uncorrected.

### 4.2. General synthesis of BAPs and PPMs

**BAPs:** In a 100 mL beaker, **1** (3.02 g, 0.02 mol) and **2** (4.87 g, 0.04 mol) were dissolved in 30 mL of acetic acid. After aerated with dry HCl gas for 1.0 hour, the mixture was stirring for 2 days at room temperature. The reaction was monitored by TLC (DCM/MeOH, 10:1, v/v). After the reaction is completed, the precipitate as intermediate **3** was filtered and was used directly for next reaction without treatment.

The intermediate **3** (0.68 g, 2.0 mmol) and benzenesulfonyl chloride (2.0 mmol) were dissolved with 100 mL of DCM. After adding 6 drops of pyridine, the mixture was stirred at room temperature overnight. The reaction endpoint was monitored by TLC. The reaction solution was washed twice with 2 mol/L hydrochloric acid, dried over anhydrous sodium sulfate, and concentrated under reduced pressure to obtain the yellow solid which was recrystallized with DCM/MeOH (1:1, v/v) to get yellow crystals of BAPs.

**PPMs:** The intermediate products BAPs (2.0 mmol), guanidine hydrochloride (0.58 g,

6.0 mmol) and potassium hydroxide (0.34 g, 6.0 mmol) were dissolved in EDC and EtOH solution (30 mL, 1:1, v/v). The mixture were heated to reflux for about 1.5~3.0 h, and monitored by TLC. The system was filtered and the filtrate was removal of the solvent under vacuum, the residue was purified on silica gel by using column using DCM and MeOH as the eluent to afford white powders PPMs.

#### 4.3. Single-Crystal Structure Determination of PPM 49

Suitable single crystals of PPM **49** were prepared by recrystallization via solvent evaporation in DCM and MeOH solution under ambient condition. It measured at 100 K with Cu K $\alpha$  radiation ( $\lambda = 1.54178 \text{ \AA}$ ) using a Rigaku OD SuperNova Dual source diffractometer with an AtlasS2 detector. Absorption was corrected for by multi-scan methods [41]. The structure was solved by direct methods and refined on  $F^2$  by full-matrix least-squares methods with SHELXL-2017/1. Crystal data of **49**: C<sub>26</sub>H<sub>23</sub>F<sub>2</sub>N<sub>4</sub>O<sub>2</sub>S·CH<sub>4</sub>O·Cl,  $M = 561.03$ , monoclinic, space group  $P21$ , clear light yellow plate,  $a = 12.2582(6) \text{ \AA}$ ,  $b = 8.3935(3) \text{ \AA}$ ,  $c = 14.2842(7) \text{ \AA}$ ,  $\beta = 115.353(6)^\circ$ ,  $V = 1328.14(12) \text{ \AA}^3$ ,  $Z = 2$ ,  $D_c = 1.403 \text{ g}\cdot\text{cm}^{-3}$ ,  $\mu(\text{Cu-K}\alpha) = 2.448 \text{ mm}^{-1}$ ,  $T = 100(2) \text{ K}$ . 1249 unique reflections [ $R_{\text{int}} = 0.0679$ ]. Final  $R_1$  [with  $I > 2\sigma(I)$ ] = 0.0550,  $wR_2$  (all data) = 0.1422. CCDC 1995582 (**49**) contains the supplementary crystallographic data for this paper. Copies of the data can be obtained free of charge on application to CCDC, 12 Union Road, Cambridge CB2 1EZ, UK (fax: (+44)1223-336-033; e-mail: [deposit@ccdc.cam.ac.uk](mailto:deposit@ccdc.cam.ac.uk)).

#### 4.4. In vitro cytotoxicity testing with MTT method

Human hepatocellular carcinoma cell lines (HepG2, SMMC-7721) and human normal heptical cell lines (HHL-5, LO2) were screened by BAPs and PPMs using a modified MTT assay (Dojindo Laboratories, Tokyo, Japan). The cells were maintained at 37 °C, 5% humidified CO<sub>2</sub> and 95% atmosphere. The HepG2 cell line was cultured in a DMEM environment containing 10% serum, and other cells were cultured in an 1640 environment containing 10% serum. First, cells were seeded at a density of  $8 \times 4$  cells/well in a 96-well plate in 200  $\mu\text{L}$  of medium per well, and cultured for 24 hours. The cells were then treated with successive concentrations of compounds (10, 5, 2.5, 1.25, 0.625, 0.3125  $\mu\text{g/mL}$ ) and incubated in an incubator for 24 hours. The control group used cells with only culture

medium as a control. After the media removed, 20  $\mu\text{L}$  of MTT (5 mg/mL) was added and cells were incubated for 4 h at 37  $^{\circ}\text{C}$ . Then, the media with MTT was removed and the dark-blue formazan crystals were dissolved by 150  $\mu\text{L}$  of DMSO. The optical density (OD) was measured at 570 nm using a multi-well plate reader (TECAN, Männedorf, Switzerland). GraphPad Prism 5 software was used to calculate their  $\text{IC}_{50}$  values. The  $\text{IC}_{50}$  value is the average of three replicates. Doxorubicin (DOX) was used as a positive control using concentrations of 5, 2.5, 1.25, 0.625, 0.3125, 0.15625  $\mu\text{g}/\text{mL}$ .

#### ***4.5. Anti-inflammatory testing of BAPs and PPMs***

In order to better discover the anti-inflammatory effects of BAPs and PPMs, we tested by inhibiting the secretion of TNF- $\alpha$  and IL-6. All BAPs and PPMs had no obvious toxicity to mouse RAW264.7 macrophages at 5.0  $\mu\text{M}$  in our pre-experiments (Supporting Information). Under the stimulation of LPS (1.0  $\mu\text{g}/\text{mL}$ ), the release of TNF- $\alpha$  and IL-6 was detected by RAW264.7 cells. After cells were treated with BAPs (5.0  $\mu\text{M}$ ) and LPS (1.0  $\mu\text{g}/\text{mL}$ ), the release of TNF- $\alpha$  and IL-6 in the medium was measured using an ELISA kit (eBioScience, San Diego, California), respectively. In simple terms, cells were pretreated with pyrrolidine dithiocarbamate (PDTC, 30  $\mu\text{M}$ ), BAPs (5.0  $\mu\text{M}$ ), or PPMs (5  $\mu\text{M}$ ) for 2h, respectively, then treated with LPS (1.0  $\mu\text{g}/\text{mL}$ ) for 22 h, and the culture medium was centrifuged at 1000 rpm for 10 minutes and determined the expression levels of TNF- $\alpha$  and IL-6 by ELISA. The inhibition rates are the means of three replicates.

#### ***4.6. Apoptosis assay***

HepG2, SMMC-7721 were seeded in a 12-well plate at a density of  $2 \times 10^5$  cells / well. After treatment with **43** (1.0, 2.0, and 4.0  $\mu\text{M}$ ) and DMSO for 24 h, cells were collected, washed twice with pre-chilled PBS, and suspended in a buffer at a concentration of  $1 \times 10^5$  cells/mL. 100  $\mu\text{L}$  of buffer was then mixed with 5  $\mu\text{L}$  of Annexin V-FITC and 5  $\mu\text{L}$  of Propidium Iodide (BD Biosciences, San Jose, CA, USA). The solution was vortexed and incubated at room temperature in the dark for 15 minutes, and apoptosis analysis was performed by flow cytometry (BD FACS Calibur).

#### ***4.6. Western blot assay***

Primary antibodies (BAX, cleaved caspase-3, Bcl-2, I $\kappa$ B $\alpha$ , phospho-I $\kappa$ B $\alpha$ , p65, phospho-p65, Akt, phospho-Akt, ERK1/2, phospho-ERK1/2, JNK, phospho-JNK, p38, phospho-p38, and GAPDH), and secondary antibodies were purchased from Cell Signaling Technology (Danvers, MA). HepG2 cells were incubated with **43** (1.0, 2.0, 4.0  $\mu$ M) for 24 h (BAX, Cleaved caspase-3, Bcl-2). RAW264.7 cells were incubated with **43** for 1 h, then RAW264.7 cells were treated with LPS (1.0  $\mu$ g/mL) for 30 minutes and then subjected to cell extraction. The cell extracts were used for Western blot analysis. Electrophoresis show protein bands, then transfer to nitrocellulose membrane, use anti-BAX, anti-cleaved caspase-3, anti-Bcl-2, anti-I $\kappa$ B $\alpha$ , anti-phospho-I $\kappa$ B $\alpha$ , anti-p65, anti-phospho-p65, anti-Akt, anti-phospho-Akt, anti-ERK1/2, anti-phospho-ERK1/2, anti-JNK, anti-phospho-JNK, anti-p38, anti-phospho-p38 or anti-GAPDH at 4 $^{\circ}$ C overnight. At room temperature, the membrane was incubated for 2 h with anti-mouse/rabbit IgG, and the expression of each protein in the membrane was detected by the ECL Western blot detection system (ChemiDoc<sup>TM</sup>XRS, Bio-Rad). Western blots were quantified from more than three separate experiments using Quantity One software (Bio-Rad).

#### ***4.7. Immunofluorescence staining***

In our study, RAW264.7 cells were cultured in 96-well plates and pretreated with LPS (1  $\mu$ g/mL) for 15 min and further with **43** for 2 h. HepG2 cells were cultured with TNF- $\alpha$  (10 ng/mL) for 15 min and further with **43** for 2 h. Next, cells were washed and fixed at room temperature. After blocked with 3% BSA, cells were incubated in turn with primary anti-p65 antibody (1:200) over night at 4  $^{\circ}$ C, and secondary antibody incubation (1:200) at room temperature for 30 min. At last, the cells were washed with PBS and incubated in DAPI for 15 min away from light. The fluorescence imaging was performed using a microscopy system in High Throughput Screen (Operetta, PerkinElmer). The p65 protein and nuclei is green and blue, respectively.

#### ***4.7. Molecular docking***

The crystal structures of Bcl-2 (PDB code: 1YSW), p65 (PDB code: 1MY5) and p38 (PDB code: 4FA2) were obtained from Protein Data Bank. Molecular docking study used LibDock

protocols of Discovery Studio 2017R2. Firstly, we generate the 3D energy minimization structure of **43**. Secondly, protein structures were optimized by adding hydrogen atoms and deleting water molecules. CHARMM force field was employed. Thirdly, after removing original ligands, optimized Bcl-2 protein was set as a receptor and placed the optimized 3D molecule of **43** in the sphere position for molecular docking. Similarly, p65 and P38 proteins are defined as receptors. The sphere was selected on the corresponding protein. And then the optimized 3D molecule of **43** was placed in the sphere position for molecular docking. The 3D and 2D models between simulated **43** and the active site of proteins were generated.

## Acknowledgements

We are grateful for financial support from the National Science Foundation of China (No. 21402010), Shandong Provincial Natural Science Foundation (No. ZR2019MB032), College Youth Innovation Science and Technology Support Program of Shandong province (No. 2020KJK003), Key R&D Program of Shandong province (No. 2019JZZY011104) and technology project of Yantai (No. 2018XSCC048).

## References

- [1] F. Bray, J. Ferlay, I. Soerjomataram, R.L. Siegel, L.A. Torre, A. Jemal, Global cancer statistics 2018: GLOBOCAN estimates of incidence and mortality worldwide for 36 cancers in 185 countries. *CA Cancer J. Clin.* 68 (2018) 394-424.
- [2] W. Chen, K. Sun, R. Zheng, H. Zeng, S. Zhang, C. Xia, Z. Yang, H. Li, X. Zou, J. He. Cancer incidence and mortality in China, 2014. *Chin. J. Cancer Res.* 30 (2018) 1-12.
- [3] C. Berasain, J. Castillo, M.J. Perugorria, M.U. Latasa, J. Prieto, M.A. Avila, Inflammation and liver cancer: New molecular links. *Ann. N. Y. Acad. Sci.* 1155 (2009) 206-221.
- [4] T. Liu, L. Zhang, D. Joo, S.C. Sun, NF- $\kappa$ B signaling in inflammation. *Signal Transduct Target Ther.* 2 (2017) 17023.
- [5] G. He, M. Karin, NF- $\kappa$ B and STAT3-key players in liver inflammation and cancer. *Cell Res.* 21 (2011) 159-168.
- [6] B. Hoesel, J.A. Schmid, The complexity of NF- $\kappa$ B signaling in inflammation and cancer. *Mol. Cancer* 12 (2013) 86.

- [7] M.S. Hayden, S. Ghosh, Shared principles in NF- $\kappa$ B signaling. *Cell* 132 (2008) 344–362.
- [8] Y. Kimura, N. Nagai, N. Tsunekawa, M. Satomatsushita, T. Yoshimoto, D.J. Cua, Y. Iwakura, H. Yagita, F. Okada, H. Tahara, I. Saiki, T. Irimura, Y. Hayakawa, IL-17A-producing CD30<sup>+</sup> V $\sigma$ 1 T cells drive inflammation-induced cancer progression. *Cancer Sci.* 107 (2016) 1206-1214.
- [9] A.A. Beg, W.C. Sha, R.T. Bronson, S. Ghosh, D. Baltimore, Embryonic lethality and liver degeneration in mice lacking the RelA component of NF- $\kappa$ B. *Nature* 376 (1995) 167–170.
- [10] Y. Xia, S. Shen, I.M. Verma, NF- $\kappa$ B, an active player in human cancers. *Cancer Immunol. Res.* 2 (2014) 823-830.
- [11] J.F. Sun, G.G. Hou, F. Zhao, W. Cong, H.J. Li, W.S. Liu, C.H. Wang, Synthesis, antiproliferative, and multidrug resistance reversal activities of heterocyclic  $\alpha,\beta$ -unsaturated carbonyl compounds. *Chem. Biol. Drug. Des.* 88 (2016) 534-541.
- [12] L. Zhang, L. Shi, S.M. Soars, J. Kamps, H. Yin, Discovery of novel small-molecule inhibitors of NF- $\kappa$ B signaling with antiinflammatory and anticancer properties. *J. Med. Chem.* 61 (2018) 5881-5899.
- [13] L. Chen, Q. Li, B. Weng, J. Wang, Y. Zhou, D. Cheng, T. Sirirak, P. Qiu, J. Wu, Design, synthesis, anti-lung cancer activity, and chemosensitization of tumor-selective MCACs based on ROS-mediated JNK pathway activation and NF- $\kappa$ B pathway inhibition. *Eur. J. Med. Chem.* 151 (2018) 508-519.
- [14] K.M. Nelson, J.L. Dahlin, J. Bisson, J. Graham, G.F. Pauli, M.A. Walters, The essential medicinal chemistry of curcumin. *J. Med. Chem.* 60 (2017) 1620-1637.
- [15] A. Olivera, T.W. Moore, F. Hu, A.P. Brown, A. Sun, D.C. Liotta, J.P. Snyder, Y. Yoon, H. Shim, A.I. Marcus, A.H. Miller, T.W. W. Pace, Inhibition of the NF- $\kappa$ B signaling pathway by the curcumin analog, 3,5-bis(2-pyridinylmethylidene)-4-piperidone (EF31): anti-inflammatory and anti-cancer properties. *Int. Immunopharmacol.* 12 (2012) 368-377.
- [16] H.P. Zhu, T.T. Xu, C.Y. Qiu, B.B. Wu, Y.L. Zhang, L.F. Chen, Q.Q. Xia, C.L. Li, B. Zhou, Z.G. Liu, G. Liang, Synthesis and optimization of novel allylated mono-carbonyl analogs of curcumin (MACs) act as potent anti-inflammatory agents against LPS-induced acute lung injury (ALI) in rats. *Eur. J. Med. Chem.* 121 (2016) 181-193.
- [17] B.R. Yao, Y. Sun, S.L. Chen, H.D. Suo, Y.L. Zhang, H. Wei, C.H. Wang, F. Zhao, W.

- Cong, W.Y. Xin, G.G. Hou, Dissymmetric pyridyl-substituted 3,5-bis(arylidene)-4-piperidones as anti-hepatoma agents by inhibiting NF- $\kappa$ B pathway activation, *Eur. J. Med. Chem.* 167 (2019) 187-199.
- [18] N. Li, W.Y. Xin, B.R. Yao, W. Cong, C.H. Wang, G.G. Hou, N-phenylsulfonyl-3,5-bis(arylidene)-4-piperidone derivatives as activation NF- $\kappa$ B inhibitors in hepatic carcinoma cell lines. *Eur. J. Med. Chem.* 155 (2018) 531-544.
- [19] N. Li, W.Y. Xin, B.R. Yao, C.H. Wang, W. Cong, F. Zhao, H.J. Li, Y. Hou, Q.G. Meng, G.G. Hou, Novel dissymmetric 3,5-bis(arylidene)-4-piperidones as potential antitumor agents with biological evaluation in vitro and in vivo. *Eur. J. Med. Chem.* 147 (2018) 21-33.
- [20] B.R. Yao, N. Li, C.H. Wang, G.G. Hou, Q.G. Meng, K. Yan, Novel asymmetric 3,5-bis(arylidene)piperidin-4-one derivatives: synthesis, crystal structures and cytotoxicity. *Acta Cryst. C74* (2018) 659–665.
- [21] N. Li, X.Y. Bai, L.S. Zhang, Y. Hou, Synthesis, crystal structures and anti-inflammatory activity of four 3,5-bis(arylidene)-N-benzenesulfonyl-4-piperidone derivatives. *Acta Cryst. C74* (2018) 1171–1179.
- [22] L.S. Zhang, Q. Chen, G.G. Hou, W. Zhao, Y. Hou, Hydroxyl-substituted double Schiff-base condensed 4-piperidone/cyclohexanones as potential anticancer agents with biological evaluation, *J. Enzyme Inhib. Med. Chem.* 34 (2019) 264-271.
- [23] C.M. Su, G.G. Hou, C.H. Wang, H.Q. Zhang, C. Yang, M. Liu, Y. Hou, Potential multifunctional agents with antihepatoma and anti-inflammation properties by inhibiting NF- $\kappa$ B activation. *J. Enzyme Inhib. Med. Chem.* 34 (2019) 1287-1297.
- [24] A.C. Pippione, I.M. Carnovale, D. Bonanni, M. Sini, P. Goyal, E. Marini, K. Pors, S. Adinolfi, D. Zonari, C. Festuccia, W. Y. Wahlgren, R. Friemann, R. Bagnati, D. Boschi, S. Oliaro-Bosso, M.L. Lolli, Potent and selective aldo-keto reductase 1C3 (AKR1C3) inhibitors based on the benzoisoxazole moiety: application of a bioisosteric scaffold hopping approach to flufenamic acid. *Eur. J. Med. Chem.* 150 (2018) 930-945.
- [25] N. Blaquiere, G.M. Castanedo, J.D. Burch, L.M. Berezhkovskiy, H. Brightbill, S. Brown, C. Chan, P.C. Chiang, J.J. Crawford, T. Dong, P. Fan, J. Feng, N. Ghilardi, R. Godemann,

- E. Gogol, A. Grabbe, A.J. Hole, B. Hu, S.G. Hymowitz, M.H.A. Ismaili, H. Le, P. Lee, W. Lee, X. Lin, N. Liu, P.A. McEwan, B. McKenzie, H.L. Silvestre, E. Suto, S. Sujatha-Bhaskar, G. Wu, L.C. Wu, Y. Zhang, Z. Zhong, S.T. Staben, A scaffold-hopping approach to discover potent, selective, and efficacious inhibitors of NF- $\kappa$ B inducing kinase. *J. Med. Chem.* 61 (2018) 6801-6813.
- [26] N. Brown, Bioisosteres and scaffold hopping in medicinal chemistry. *Mol. Inform.* 33 (2014) 458-462.
- [27] K. Arvind, I. Hiriyakkanavar, J. Hiriyakkanavar, Ketene dithioacetals. Part 11. Reaction of 3-cyano-4-methylthio-2(1H)-pyridones with hydrazine and guanidine: synthesis of novel substituted and fused pyrazolo[4,3-c]pyridone and pyrido[4,3-d]pyrimidine derivatives. *J. Chem. Soc. Perkin Trans 1.* 8 (1978) 857-862.
- [28] J.B. Sainani, A.C. Shah, V.P. Arya, Formation of 1,4,5,6,7,8-hexahydro-pyrido(4,3-d)pyridine by hantzsch synthesis. *Indian J. Chem. B* 33 (1994) 526-531.
- [29] S. Rostamizadeh, N. Shadjou, E. Isapoor, M. Hasanzadeh, Catalytic activity of (Fe<sub>2</sub>O<sub>3</sub>)-MCM-41-nPrNH<sub>2</sub> magnetically recoverable nanocatalyst for the synthesis of phenylpyrido[4,3-d]pyrimidins. *J. Nanosci. Nanotechnol.* 13 (2013) 4925-4933.
- [30] A.M. Mohamed, W.A. El-Sayed, M.A. Alsharari, H.R.M. Al-Qalawi, M.O. Germoush, Anticancer activities of some newly synthesized pyrazole and pyrimidine derivatives. *Arch. Pharm. Res.* 36 (2013) 1055-1065.
- [31] Y. Sun, Z.F. Gao, C.H. Wang, G.G. Hou, Synthesis, crystal structures and anti-inflammatory activity of fluorine-substituted 1,4,5,6-tetrahydrobenzo[h]quinazolin-2-amine derivatives. *Acta Cryst. C* 75 (2019) 1157-1165.
- [32] D.L. Yin, Y.J. Liang, T.S. Zheng, R.P. Song, J.B. Wang, B.S. Sun, S.H. Pan, L.D. Qu, J.R. Liu, H.C. Jiang, L.X. Liu, EF24 inhibits tumor growth and metastasis via suppressing NF- $\kappa$ B dependent pathways in human cholangiocarcinoma. *Sci. Rep.* 6 (2016) 32167.
- [33] D. Subramaniam, R. May, S.M. Sureban, K.B. Lee, R. George, P. Kuppusamy, R.P. Ramanujam, K. Hideq, B.K. Dieckgraefe, C.W. Houchen, S. Anant, Diphenyl

- Difluoroketone: A Curcumin Derivative with Potent In vivo Anticancer Activity. *Cancer Res.* 68 (2008) 1962-1969.
- [34] V. Gouverneur, K. Müller, *Fluorine in pharmaceutical and medicinal chemistry*[M]. 2012.
- [35] C.S. Jiang, C.L. Zhuang, K. Zhu, J. Zhang, L.A. Muehlmann, J.P.F. Longo, R.B. Azevedo, W. Zhang, N. Meng, H. Zhang, Identification of a novel small-molecule Keap1-Nrf2 PPI inhibitor with cytoprotective effects on LPS-induced cardiomyopathy, *J. Enzyme Inhib. Med. Chem.* 33 (2018) 833-841.
- [36] C.L. Gao, G.G. Hou, J. Liu, T. Ru, Y.Z. Xu, S.Y. Zhao, H. Ye, L.Y. Zhang, K.X. Chen, Y.W. Guo, T. Pang, X.W. Li, Synthesis and target identification of benzoxepane derivatives as potential anti-neuroinflammatory agents for ischemic stroke. *Angew. Chem. Int. Ed.* 59 (2020) 2429-2439.
- [37] X.S. Liu, H. Zou, C. Slaughter, X.D. Wang, DFF, a heterodimeric protein that functions downstream of Caspase-3 to trigger DNA fragmentation during apoptosis. *Cell*, 89 (1997) 175-184.
- [38] R.J. Davis, Mapks: New JNK expands the group. *Trends in Biochemical Sciences*, 19 (1994) 470-473.
- [39] C.S. Jiang, Y.X. Ge, Z.Q. Cheng, J.L. Song, Y.Y. Wang, K.K. Zhu, H. Zhang, Discovery of new multifunctional selective acetylcholinesterase inhibitors: Structure-based virtual screening and biological evaluation. *J. Comput. Aided. Mol. Des.* 33 (2019) 521–530.
- [40] G.G. Hou, H.J. Zhao, J.F. Sun, D. Lin, X.P. Dai, J.T. Han, H. Zhao, Synthesis, structure and luminescence of Co-crystals with hexagonal channels: arranging disposition and  $\pi$ - $\pi$  interactions. *CrystEngComm*, 15 (2013) 577-585.
- [41] Rigaku OD (2015). *CrysAlis PRO*. Rigaku Oxford Diffraction Ltd, Yarnton, Oxfordshire, England.

**Table 1** Cytotoxicity of BAPs (**4-30**) and DOX.

**Table 2** Cytotoxicity of PPMs (**31-57**) and DOX.

**Table 3** Anti-inflammatory activity of PPMs (**31-57**) against inflammatory response in LPS-stimulated RAW264.7 cell.

**Scheme 1** The synthetic routes of BAPs and PPMs.

**Fig. 1.** The scaffold hopping strategy of PPMs.

**Fig. 2.** (A)  $^1\text{H}$ NMR spectrum and proton attribution of **17**; (B)  $^1\text{H}$ NMR spectrum and proton attribution of **44**; (C)  $^{13}\text{C}$ NMR spectrum and carbon attribution of **17**; (D)  $^{13}\text{C}$ NMR spectrum and carbon attribution of **44**.

**Fig. 3.** (A) The ORTEP figure of **49** (Displacement ellipsoids with 30% probability). (B) Some BAPs reported in the literatures.

**Fig. 4.** (A) The structure of PPM **43**. (B) Cell apoptotic of HepG2 and SMMC-7721 by **43** through flow cytometry. (C) The expression of BAX, Bcl-2, and cleaved caspase-3 in HepG2 cells was determined by western blotting. Western blots were quantified from more than three separate experiments (\* $P < 0.05$ , \*\*  $P < 0.01$ , \*\*\*  $P < 0.001$  compared to DMSO group).

**Fig. 5.** (A) Inhibitory effects of **43** on LPS-stimulated phosphorylation of p65 (B), I $\kappa$ B $\alpha$  (C) and Akt (D) in RAW264.7 cells, respective. They were detected by Western blotting. GAPDH was used as a control. Data represent the mean  $\pm$  SD of triplicate tests. \* $P < 0.05$ , \*\* $P < 0.01$ , \*\*\* $P < 0.001$  compared with LPS group. ### $P < 0.001$  compared with DMSO group.

**Fig. 6.** (A) Inhibitory effects of **43** on LPS-induced MAPK signaling in RAW264.7 cells detected by Western blotting. (B-D) Inhibitory effects of **43** on LPS-induced phosphorylation of p38 (B), ERK (C) and JNK (D), respective. GAPDH was used as a control. Data represent the mean  $\pm$  SD of triplicate tests. \* $P < 0.05$ , \*\* $P < 0.01$ , \*\*\* $P < 0.001$  compared with LPS

group.  $^{###}P < 0.001$  compared with DMSO group.

**Fig. 7.** Effects of **43** on the nuclear translocation of NF- $\kappa$ B p65 protein in the LPS-stimulated RAW264.7 cells (A) or TNF- $\alpha$ -stimulated HepG2 cells (B) by immunofluorescence assay.

These experiments were repeated three times with similar results.

**Fig. 8.** 3D model and 2D model of the interaction between simulated **43** and the active site of Bcl-2 (A), p65 (B), and p38 (C) proteins.

Journal Pre-proof

**Table 1**Cytotoxicity of BAPs (**4-30**) and DOX.

No.	R <sub>1</sub>	R <sub>2</sub>	IC <sub>50</sub> (μM) of cytotoxicity			
			HepG2	SMMC-7721	HHL-5	LO2
<b>4</b>	2-F	-H	15.9±0.1	5.7±0.6	27.2±0.5	17.6±0.1
<b>5</b>	2-F	-CH <sub>3</sub>	14.2±0.5	4.1±0.1	7.9±0.4	16.7±0.1
<b>6</b>	2-F	-NO <sub>3</sub>	16.5±0.4	6.2±0.4	6.6±1.2	15.5±0.2
<b>7</b>	2-F	-CF <sub>3</sub>	4.9±0.2	5.2±0.5	15.3±0.4	16.2±0.1
<b>8</b>	2-F	-F	8.0±0.6	7.7±0.7	14.5±0.5	17.5±0.4
<b>9</b>	2-F	-Cl	10.9±0.1	4.5±0.3	9.6±1.1	14.1±0.2
<b>10</b>	2-F	-Br	13.7±0.1	5.2±0.7	14.0±0.2	16.2±0.1
<b>11</b>	2-F	-CN	16.5±0.7	14.6±0.5	13.6±0.5	11.0±1.2
<b>12</b>	2-F	-NHAc	5.2±0.4	7.5±0.3	13.6±0.9	11.5±0.1
<b>13</b>	3-F	-H	3.4±0.2	12.9±0.2	17.1±0.2	16.2±0.2
<b>14</b>	3-F	-CH <sub>3</sub>	3.5±0.8	18.1±0.5	11.2±0.2	15.7±1.1
<b>15</b>	3-F	-NO <sub>3</sub>	8.1±0.5	15.3±0.5	14.5±0.3	10.7±0.1
<b>16</b>	3-F	-CF <sub>3</sub>	2.4±0.2	4.2±0.2	13.4±0.7	18.0±1.1
<b>17</b>	3-F	-F	5.0±0.2	13.5±0.4	15.4±0.2	21.9±0.1
<b>18</b>	3-F	-Cl	13.1±0.8	7.8±0.2	10.8±0.5	15.7±0.2
<b>19</b>	3-F	-Br	7.7±0.6	11.7±0.3	16.5±0.2	15.8±0.2
<b>20</b>	3-F	-CN	2.6±0.4	4.5±0.6	7.5±0.3	15.5±0.1
<b>21</b>	3-F	-NHAc	11.1±0.6	10.3±0.8	17.0±0.3	17.5±0.1
<b>22</b>	4-F	-H	18.8±0.3	9.1±0.3	7.7±0.3	18.8±0.3
<b>23</b>	4-F	-CH <sub>3</sub>	4.5±0.1	5.0±0.6	6.0±0.4	14.0±0.3
<b>24</b>	4-F	-NO <sub>3</sub>	5.4±0.2	5.0±0.6	7.8±0.5	16.2±1.4
<b>25</b>	4-F	-CF <sub>3</sub>	3.2±0.4	4.4±0.3	16.1±0.3	13.5±0.3
<b>26</b>	4-F	-F	8.1±0.3	14.7±0.5	11.7±0.2	14.8±0.3
<b>27</b>	4-F	-Cl	4.5±0.4	7.0±0.3	17.7±0.6	15.5±0.6
<b>28</b>	4-F	-Br	8.0±0.6	11.5±0.4	17.1±0.5	16.4±1.4
<b>29</b>	4-F	-CN	9.8±0.5	15.0±0.4	14.6±0.8	14.7±0.4
<b>30</b>	4-F	-NHAc	7.4±0.3	9.8±0.7	15.0±0.7	19.4±1.2
DOX	-	-	1.0±0.4	1.4±0.3	12.2±0.4	13.8±0.3

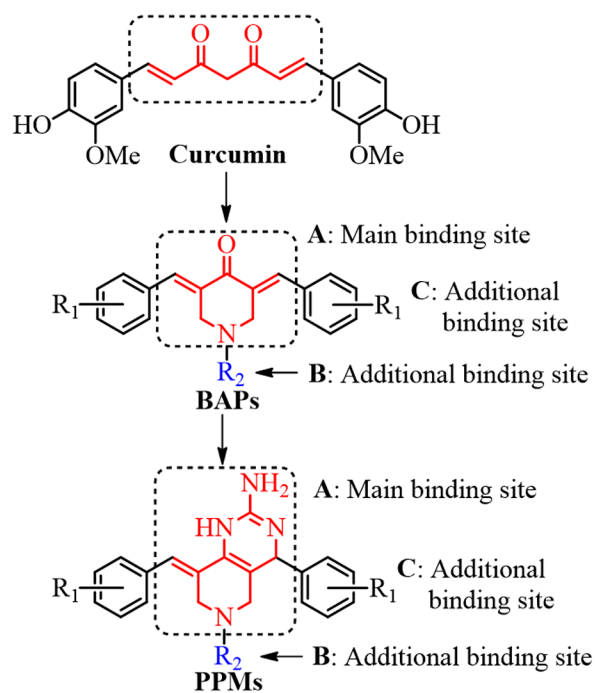
**Table 2**Cytotoxicity of PPMs (**31-57**) and DOX.

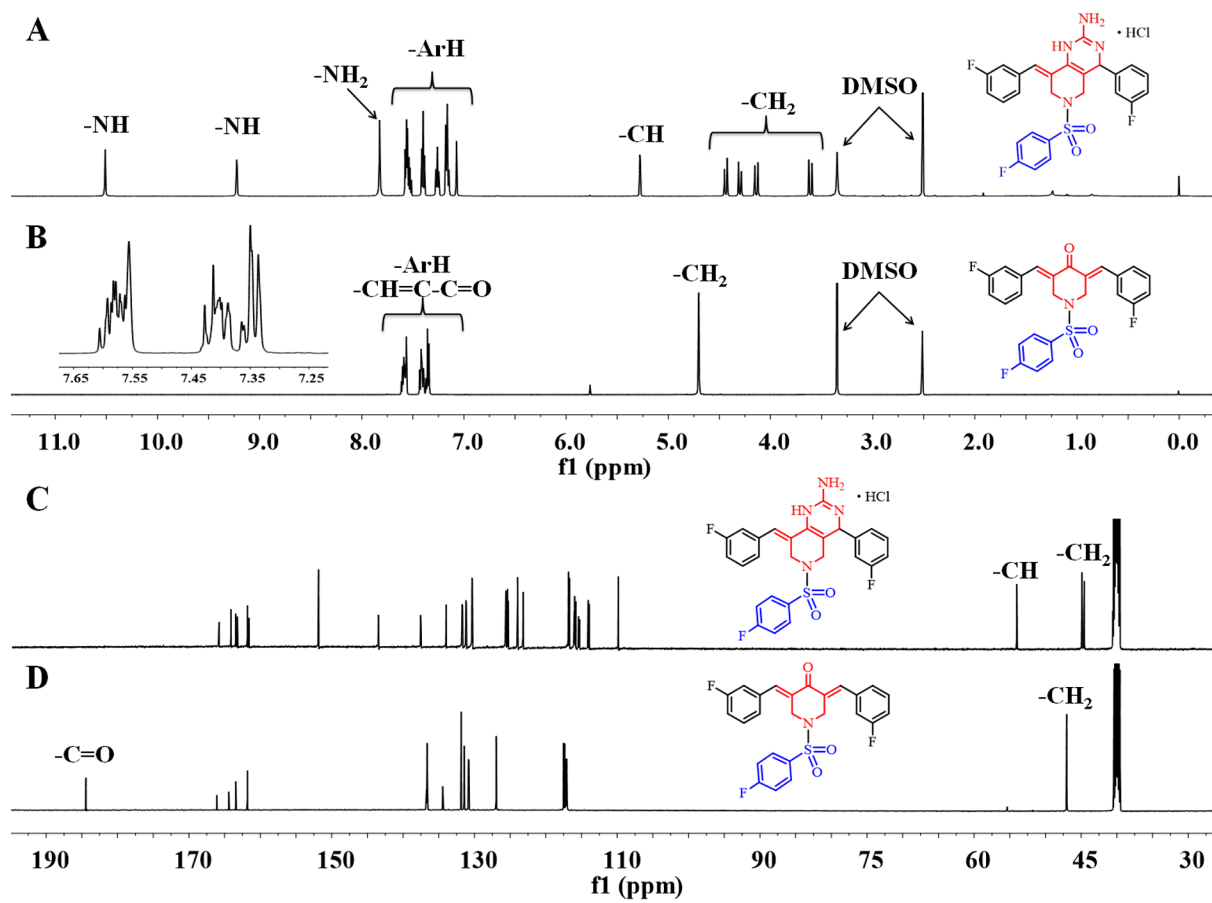
No.	R <sub>1</sub>	R <sub>2</sub>	IC <sub>50</sub> (μM) of cytotoxicity			
			HepG2	SMMC-7721	HHL-5	LO2
<b>31</b>	2-F	-H	9.9±0.5	8.5±0.2	9.9±0.4	11.2±0.1
<b>32</b>	2-F	-CH <sub>3</sub>	13.1±2.2	7.3±2.1	9.6±2.3	11.5±0.4
<b>33</b>	2-F	-NO <sub>3</sub>	11.9±0.5	5.7±0.4	10.7±0.5	12.4±0.2
<b>34</b>	2-F	-CF <sub>3</sub>	3.9±0.3	3.5±0.1	20.8±0.4	22.0±0.6
<b>35</b>	2-F	-F	12.1±0.6	10.0±0.5	12.0±0.8	16.5±0.3
<b>36</b>	2-F	-Cl	12.2±0.2	4.9±0.3	9.1±0.2	11.5±2.2
<b>37</b>	2-F	-Br	10.4±0.3	9.7±0.3	12.5±0.3	19.5±2.9
<b>38</b>	2-F	-CN	11.7±0.4	19.0±1.1	29.0±2.4	12.0±0.3
<b>39</b>	2-F	-NHAc	11.8±0.3	8.6±1.2	22.1±1.2	11.2±3.3
<b>40</b>	3-F	-H	3.7±0.2	12.8±0.5	11.3±2.3	37.8±3.3
<b>41</b>	3-F	-CH <sub>3</sub>	11.7±0.2	11.7±1.5	23.2±1.3	11.2±0.5
<b>42</b>	3-F	-NO <sub>3</sub>	30.6±0.3	12.3±0.1	30.5±0.6	42.4±5.3
<b>43</b>	3-F	-CF <sub>3</sub>	2.1±0.3	2.4±0.3	28.8±1.4	35.2±3.1
<b>44</b>	3-F	-F	12.4±0.2	4.8±0.6	12.9±0.9	18.8±2.4
<b>45</b>	3-F	-Cl	15.0±0.1	5.5±0.2	12.0±0.7	15.1±0.5
<b>46</b>	3-F	-Br	10.6±0.1	6.3±0.3	13.0±0.5	10.1±0.2
<b>47</b>	3-F	-CN	3.5±0.4	4.2±0.3	18.9±0.8	17.2±0.3
<b>48</b>	3-F	-NHAc	22.9±0.4	6.5±0.4	10.7±0.3	15.0±0.3
<b>49</b>	4-F	-H	9.5±0.3	8.0±0.2	11.5±3.3	9.9±0.1
<b>50</b>	4-F	-CH <sub>3</sub>	4.5±0.4	4.3±0.7	32.7±1.5	17.7±0.3
<b>51</b>	4-F	-NO <sub>3</sub>	9.4±0.4	19.1±0.2	10.3±0.8	12.5±0.4
<b>52</b>	4-F	-CF <sub>3</sub>	3.3±0.2	3.8±0.1	24.4±0.2	15.4±0.6
<b>53</b>	4-F	-F	4.1±0.3	17.1±0.4	11.1±0.6	13.3±0.5
<b>54</b>	4-F	-Cl	7.6±0.3	12.0±0.2	27.1±2.8	16.7±0.2
<b>55</b>	4-F	-Br	5.6±0.6	12.2±0.5	18.3±0.6	18.3±0.4
<b>56</b>	4-F	-CN	11.7±0.4	42.7±2.3	26.7±0.4	18.6±0.4
<b>57</b>	4-F	-NHAc	7.4±0.3	6.2±0.4	32.2±4.6	20.3±0.1
DOX	-	-	1.0±0.2	1.4±0.3	12.2±1.4	13.8±2.3

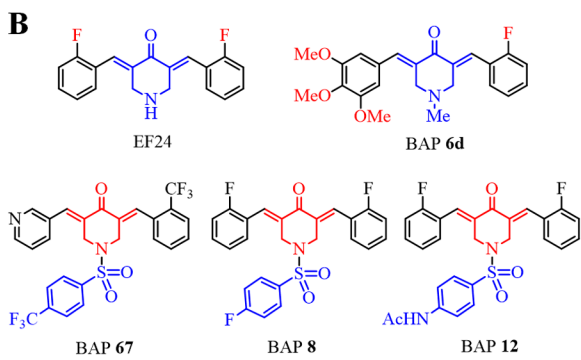
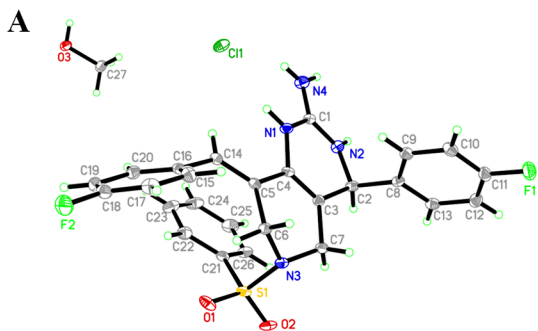
**Table 3**

Anti-inflammatory activity of PPMs (**31-57**) against inflammatory response in LPS-stimulated RAW264.7 cell.

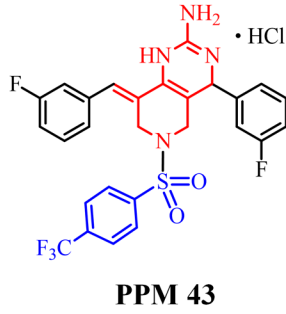
No.	Inhibition rate (%)		No.	Inhibition rate (%)	
	PPMs (5 $\mu$ M) + LPS (1 $\mu$ g/mL)			PPMs (5 $\mu$ M) + LPS (1 $\mu$ g/mL)	
	TNF- $\alpha$	IL-6		TNF- $\alpha$	IL-6
<b>31</b>	46.9 $\pm$ 1.3	40.5 $\pm$ 0.4	<b>45</b>	57.7 $\pm$ 1.4	75.9 $\pm$ 2.1
<b>32</b>	44.0 $\pm$ 1.4	56.8 $\pm$ 1.5	<b>46</b>	69.3 $\pm$ 3.2	71.0 $\pm$ 1.4
<b>33</b>	72.7 $\pm$ 2.1	79.6 $\pm$ 3.5	<b>47</b>	74.5 $\pm$ 2.4	73.0 $\pm$ 1.5
<b>34</b>	84.4 $\pm$ 1.6	82.3 $\pm$ 2.6	<b>48</b>	69.9 $\pm$ 2.4	57.5 $\pm$ 0.5
<b>35</b>	78.6 $\pm$ 1.1	79.5 $\pm$ 1.8	<b>49</b>	33.5 $\pm$ 2.1	39.8 $\pm$ 2.3
<b>36</b>	83.0 $\pm$ 0.8	81.5 $\pm$ 1.1	<b>50</b>	61.8 $\pm$ 4.0	60.1 $\pm$ 2.5
<b>37</b>	74.4 $\pm$ 3.2	79.6 $\pm$ 1.0	<b>51</b>	65.9 $\pm$ 1.3	66.8 $\pm$ 2.8
<b>38</b>	62.9 $\pm$ 2.1	71.2 $\pm$ 2.0	<b>52</b>	87.5 $\pm$ 1.9	81.7 $\pm$ 4.0
<b>39</b>	67.6 $\pm$ 2.4	61.6 $\pm$ 1.7	<b>53</b>	72.3 $\pm$ 0.8	71.4 $\pm$ 1.5
<b>40</b>	54.0 $\pm$ 1.5	56.3 $\pm$ 4.3	<b>54</b>	48.4 $\pm$ 2.4	54.8 $\pm$ 1.3
<b>41</b>	40.5 $\pm$ 3.6	46.7 $\pm$ 2.4	<b>55</b>	58.1 $\pm$ 1.3	64.3 $\pm$ 1.2
<b>42</b>	58.8 $\pm$ 1.1	78.5 $\pm$ 1.0	<b>56</b>	45.9 $\pm$ 1.4	51.1 $\pm$ 3.2
<b>43</b>	88.5 $\pm$ 0.7	86.8 $\pm$ 1.2	<b>57</b>	40.1 $\pm$ 3.2	54.2 $\pm$ 2.4
<b>44</b>	71.6 $\pm$ 0.8	74.9 $\pm$ 2.5	PDTC(30 $\mu$ M)	66.5 $\pm$ 2.3	56.9 $\pm$ 1.3
LPS	0	0			



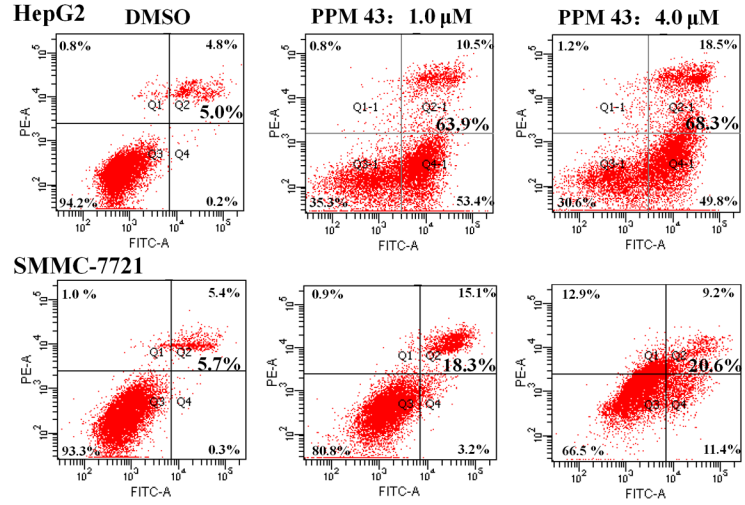




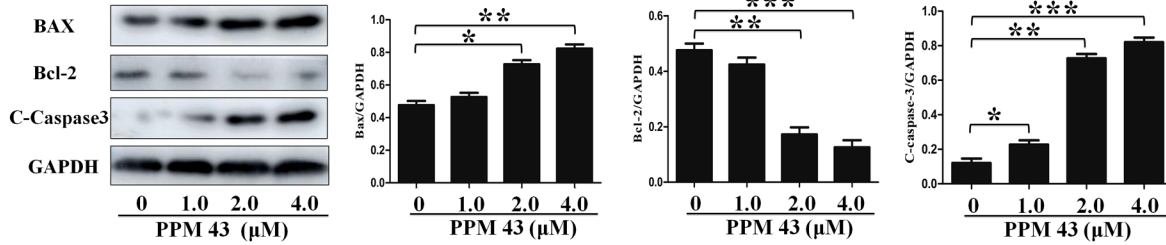
A

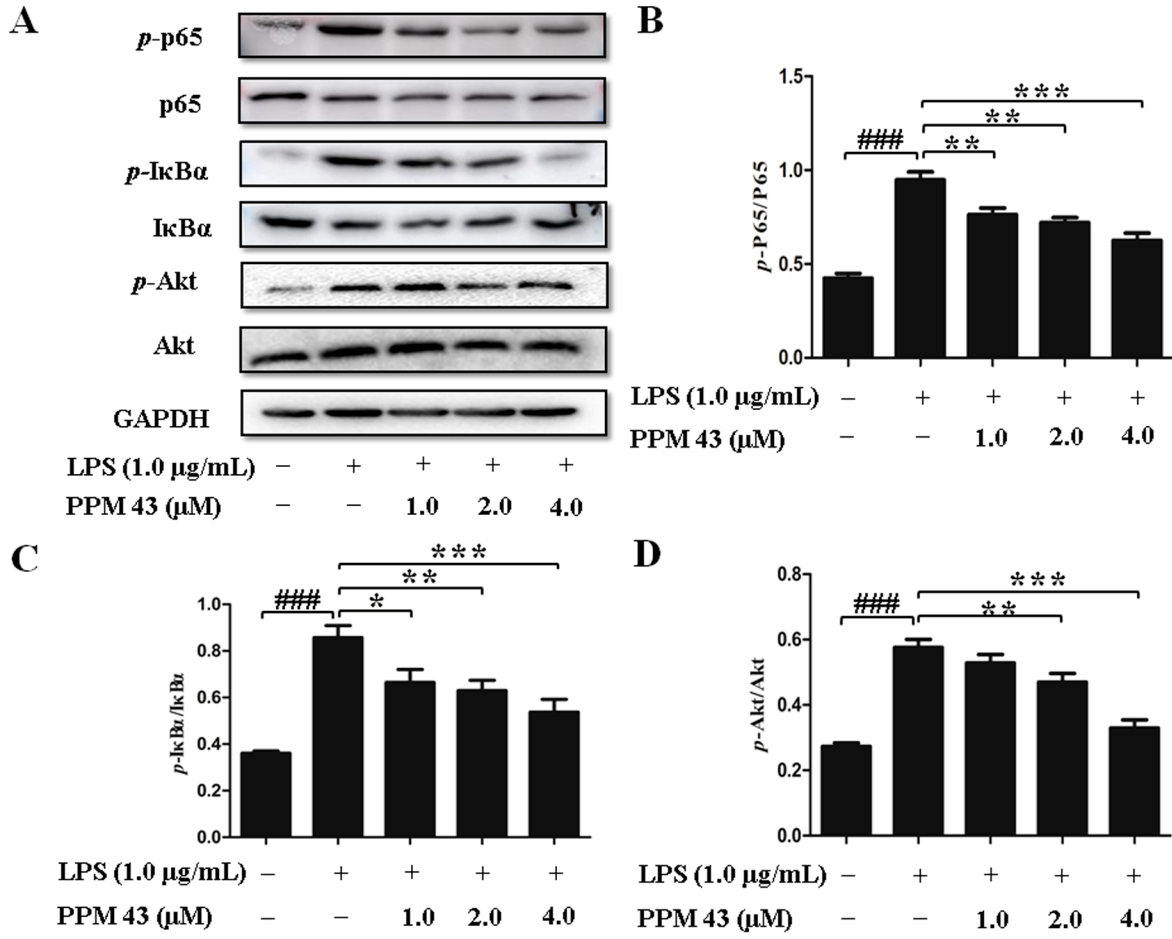


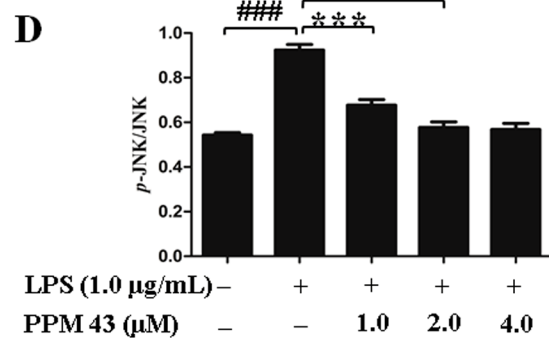
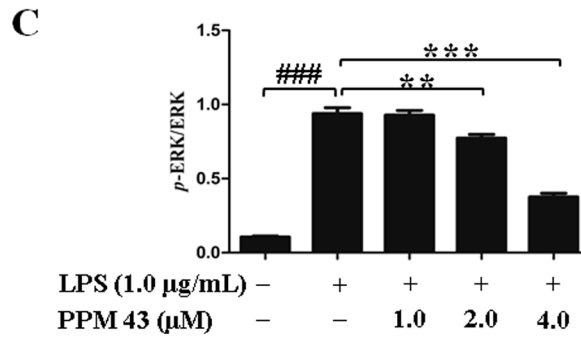
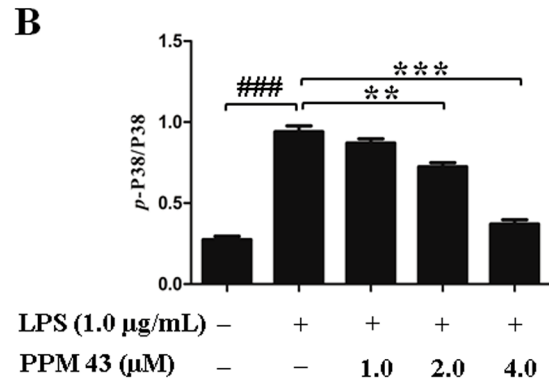
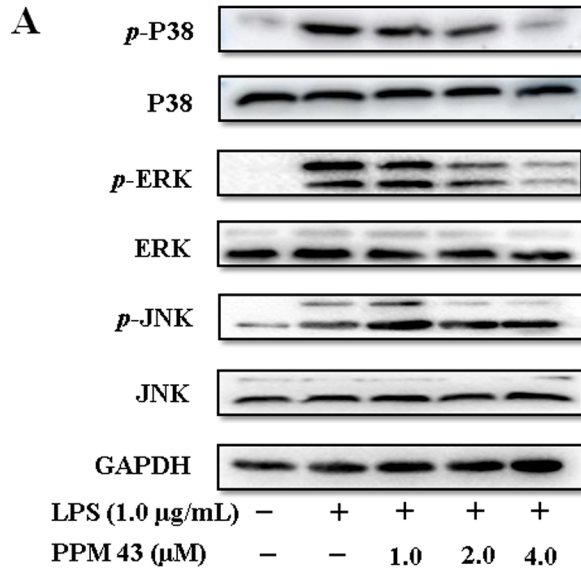
B

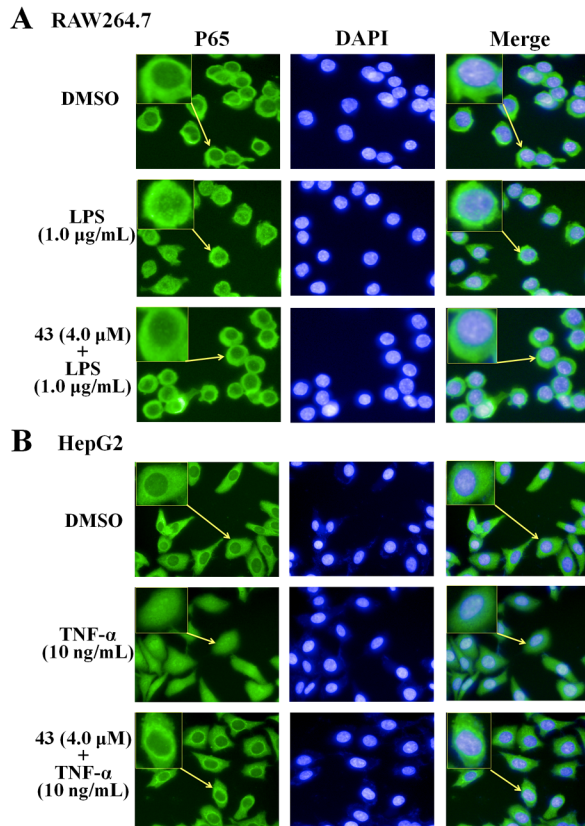


C

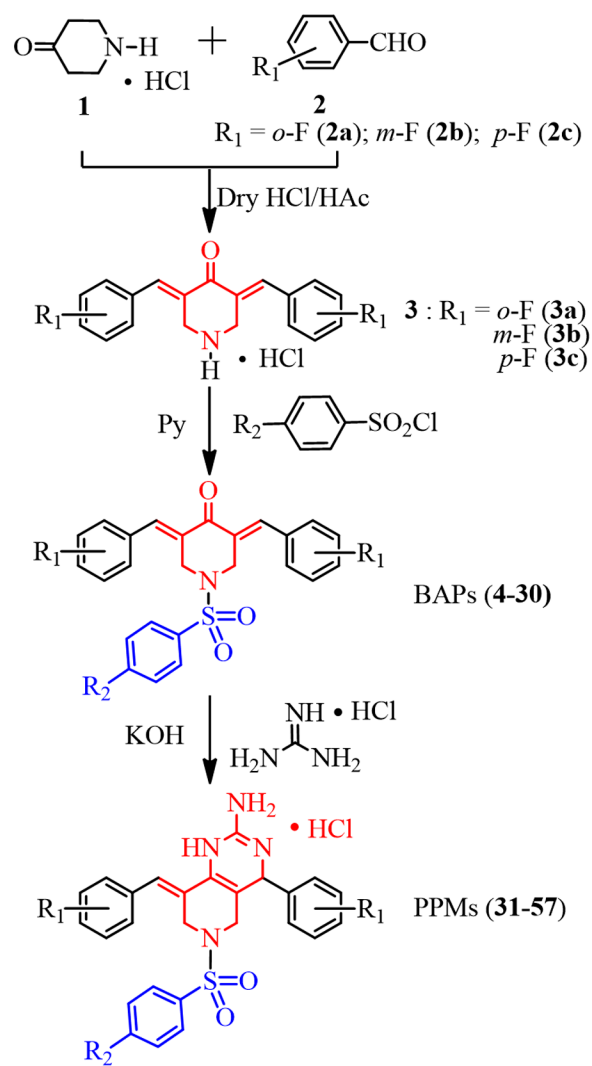












### Highlights

1. Fluoro-substituted 1,4,5,6,7,8-hexahydropyrido[4,3-*d*]pyrimidines (PPMs) were synthesized based on scaffold hopping.
2. 3-F and 4-CF<sub>3</sub>-substituted **43** exhibited less toxicity and higher anti-inflammatory activity.
3. **43** induced dose-dependent cell apoptosis at cell and protein level.
4. **43** inhibited NF- $\kappa$ B activation by suppressing LPS-induced phosphorylation levels of p65, I $\kappa$ B $\alpha$  and Akt proteins and MAPK signaling.
5. **43** inhibited NF- $\kappa$ B activation by inhibiting nuclear translocation of NF- $\kappa$ B induced by TNF- $\alpha$  or LPS.
6. **43** could bind to active site of Bcl-2, p65 and p38 proteins by molecular docking.

No potential conflict of interest was reported by the authors.

Journal Pre-proof